Current Biology 21, 1727–1731, October 25, 2011 ©2011 Elsevier Ltd All rights reserved DOI 10.1016/j.cub.2011.08.047

Report

Reconstitution of Amoeboid Motility In Vitro Identifies a Motor-Independent Mechanism for Cell Body Retraction

Katsuya Shimabukuro,[1] Naoki Noda,[2] Murray Stewart,[3] and Thomas M. Roberts[1,*]

[1]Department of Biological Science, Florida State University, Tallahassee, FL 32306, USA

[2]Marine Biological Laboratory, Woods Hole, MA 02543, USA

[3]MRC Laboratory of Molecular Biology, Hills Road, Cambridge CB2 2QH, UK

Summary

Crawling movement in eukaryotic cells requires coordination of leading-edge protrusion with cell body retraction [1–3]. Protrusion is driven by actin polymerization along the leading edge [4]. The mechanism of retraction is less clear; myosin contractility may be involved in some cells [5] but is not essential in others [6–9]. In *Ascaris* sperm, protrusion and retraction are powered by the major sperm protein (MSP) motility system instead of the conventional actin apparatus [10, 11]. These cells lack motor proteins [12] and so are well suited to explore motor-independent mechanisms of retraction. We reconstituted protrusion and retraction simultaneously in MSP filament meshworks, called fibers, that assemble behind plasma membrane-derived vesicles. Retraction is triggered by depolymerization of complete filaments in the rear of the fiber [13]. The surviving filaments reorganize to maintain their packing density. By packing fewer filaments into a smaller volume, the depolymerizing network shrinks and thereby generates sufficient force to move an attached load. Our work provides direct evidence for motor-independent retraction in the reconstituted MSP motility system of nematode sperm. This mechanism could also apply to actin-based cells and may explain reports of cells that crawl even when their myosin activity is compromised.

Results and Discussion

Generation of Major Sperm Protein Comet Tails in which Protrusion and Retraction Occur Simultaneously

Previous work demonstrated that the cytoskeletal dynamics associated with leading-edge protrusion and cell body retraction can reconstituted independently in a simple cell-free extract obtained as the 100,000 × g supernatant (S100) from lysed *Ascaris* sperm [14, 15]. For example, addition of 1 mM ATP to 5-fold diluted S100 reconstitutes leading-edge protrusion by triggering major sperm protein (MSP) polymerization behind plasma membrane-derived vesicles to form a fiber that pushes the vesicles forward as it grows (see Figure S1A and Movie S1 available online) [14]. Conversely, treatment of these fibers with YOP, a tyrosine phosphatase, causes them to disassemble and shrink (Figure S1B), recapitulating the cytoskeletal dynamics involved in cell body retraction [15, 16]. To explore the mechanism of retraction and its relationship to protrusion, we identified conditions in which both processes can be reconstituted simultaneously, but at different locations within the same fiber. By adjusting either the dilution of the extract or the concentration of added ATP, about 60% of batches of S100 could be induced to form fibers that exhibited simultaneous but spatially separated protrusion and retraction. For example, at 80% S100 and 1 mM ATP, filament assembly occurred at the surface of the membrane vesicle and pushed the vesicle forward (Figure 1A; Movie S2). At the same time, filament disassembly further rearward resulted in a gradual decrease in optical density along the length of the fiber. Addition of 50 μM ATP to 20% S100 resulted in similar behavior. These fibers maintained a nearly constant length as they moved along and exhibited a pattern very similar to that of the actin comet tails that form behind intracellular pathogens such as *Listeria* or beads coated with agents that activate assembly of dendritic actin filament arrays [17]. Therefore, we refer to fibers exhibiting this pattern as comet tail fibers.

Retraction Force Generation in Comet Tail Fibers

Often, particles in the S100 stuck to comet tails fibers. Examination of the movement of these particles showed that the disassembling part of the fiber generated sufficient force to move a load. For example, Figure 1B shows a comet tail fiber with a large dark object stuck to its trailing end. This object remained attached and was pulled forward at the same rate as growth at the opposite end of the fiber pushed the vesicle. Smaller objects stuck to fibers appeared as dark specks and could be used as fiduciary marks to chart retraction within the fiber itself. Figure 1C (see also Movie S3) shows a comet tail fiber with a speck stuck to the retracting rear region. The distance between that speck and another stuck to the substrate (near the growing end of the fiber at the start of the sequence) decreased with time as the fiber-bound speck was pulled forward. Over the same interval, elongation of the fiber pushed the vesicle at the growing end of the fiber away from the substrate-attached speck. The speck on the fiber moved with respect to the substratum while the distance between it and the vesicle at the growing end of the fiber remained nearly constant. This forward movement of specks attached to the rear of comet tail fibers demonstrated that fiber disassembly was able to perform work.

Fluorescent speckle microscopy [18] confirmed that particles attached at the rear of comet tail fibers were being pulled forward and not moving independently over the fiber. Addition of 40 nM Cy3-labeled MSP to 80% S100 resulted in the formation of comet tail fibers with fluorescent speckles (Figure 1D; Movie S4). Although many speckles at the rear of the comet tail fiber disappeared quickly, probably due to loss of fluorescent MSP subunits during filament depolymerization, several persisted long enough to chart their movement. Those near the front of the fiber remained stationary relative to the substratum as the vesicle moved away. By contrast, speckles at the rear moved forward along with the fiber. Thus, the behavior of these speckles showed that the MSP filaments themselves, like attached objects, are pulled forward by forces generated during retraction.

*Correspondence: roberts@bio.fsu.edu

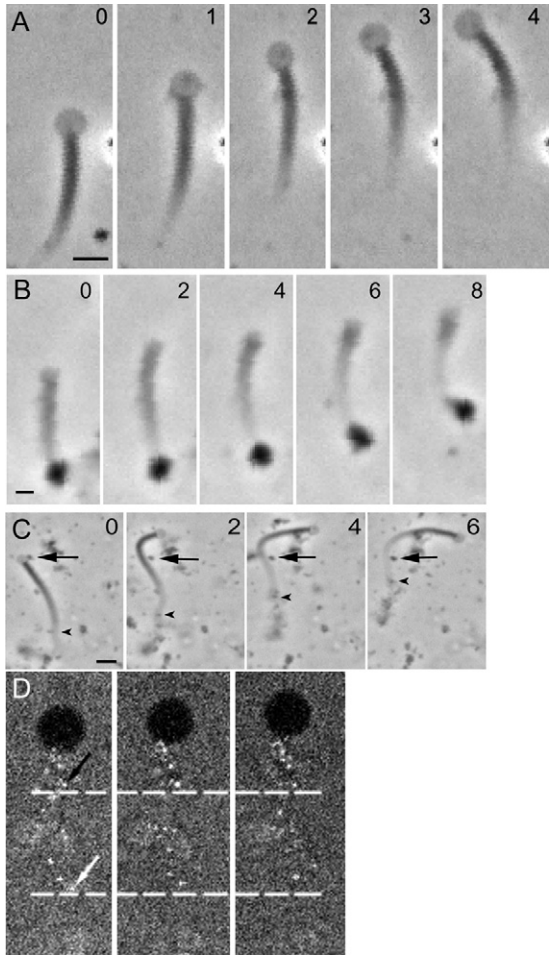

Figure 1. Comet Tail Fiber Dynamics and Force Generation

(A) Comet tail fiber in which major sperm protein (MSP) polymerizes at the front and disassembles toward the rear at about the same rate, so that the fiber maintains its length over time.

(B) Time-lapse images of a comet tail fiber with a dark piece of debris attached to its trailing end. This "cargo" is pulled forward at about the same rate as the movement of the vesicle at the opposite, growing end of the fiber.

(C) A comet tail fiber moving past a dark speck (arrow) attached to the glass. A second speck (arrowhead) attached to the rear part of the fiber is pulled forward, toward the substrate-attached speck, while the vesicle is pushed away. This pattern illustrates the simultaneous growth and shrinkage that occur in comet tail fibers.

(D) Time-lapse images taken 15 seconds apart of a comet tail fiber grown in S100 supplemented with a small amount of Cy3-MSP to produce a fluorescent speckle labeling pattern. Two horizontal white lines have been added to assist in following the movement of individual speckles. One speckle (white arrow) in the rear part of the fiber moves forward due to retraction in the region while a second (black arrow) near the vesicle remains stationary as the vesicle moves away.

Numerals indicate elapsed time in minutes in (A)–(C). Scale bars represent 2 μm in (A) and (B) and 5 μm in (C). See also Movie S1, Movie S2, Movie S3, Movie S4, and Figure S1.

The Transition from Protrusion to Retraction

Generating comet tail fibers allowed us to probe the mechanism of retraction by exploring how the filament network changed as it switched from growth at the front to retraction at the rear. We used correlative confocal fluorescence and electron microscopy to measure changes in the mass and packing density of the filament network along the length of comet tail fibers grown in the presence of Cy3-MSP (Figures 2A and 2B). The total fluorescence intensity in cross-sections generated from z stacks (Figures 2C–2E) provided an estimate of the filament mass at defined positions along the length of the fiber (Figure 2F). The same fibers were identified in platinum replicas and used to measure fiber diameter at the same positions. This allowed us to estimate filament density as the total Cy3-MSP fluorescence per unit cross-sectional area (Figure 2F). If the filament network does not reorganize during retraction, the total filament mass and packing density should decrease together. However, we found that near the rear of the fiber, where retraction was nearly complete, cross-sections retained on average only 5% of the of the total fluorescence observed at the front of the fiber but still had 45%–50% of their initial fluorescence density (Figure 2G). These data suggest that filament packing density is at least partially conserved during retraction.

Electron microscope (EM) tomography of platinum replicas of comet tail fibers confirmed this conservation of packing density. We generated tomograms at the front, middle, and rear of the fiber (Figures 3A–3D) that we then used to track and measure every filament in each tomogram (Figures 3E–3G). As expected, the number of filaments per region decreased substantially with distance from the vesicle, so that at the rear of the comet tail, where retraction was nearly complete, the number of filaments was only ~10% of that at the front where retraction had not yet started (Figure 3H). Surprisingly, the average lengths of filaments at the front and rear of the fiber were indistinguishable (Figure 3I), suggesting that whole filaments are lost in an all-or-none depolymerization, rather than by all filaments gradually shortening. Analogous catastrophic depolymerization of actin filaments has been observed in *Listeria* comet tails and in *Xenopus* egg extracts [19].

We estimated filament packing density in cross-sectional views generated from the tomograms (Figures 3E–3G) by measuring the area within the perimeter of the filament-occupied space in each region and counting the number of filaments within that perimeter. This analysis showed that although the numbers of filaments in the middle and back region were only ~40% and ~10%, respectively, of that in the front (Figure 3I), the filament packing density was similar in all three regions (Figure 3J). We were unable to identify additional platinum replicas of comet tail fibers suitable for EM tomography but did examine several comet tail fibers by conventional EM (Figures 3K–3O). The diameter of each of these fibers narrowed dramatically from the middle to the back, where depolymerization and retraction occurred, and the surviving filaments in the rear of the fiber were packed tightly, features consistent with conservation of packing density.

Filament Rearrangement during Retraction

Retracting fibers could conserve packing density either by retaining filaments in the fiber core while peripheral filaments depolymerize or by repacking the filaments that survive depolymerization to compensate for the loss of their neighbors. To discriminate between these possibilities, we examined comet tail fibers by polarization microscopy using an LC-PolScope system. This optical system produces computed images that show the magnitude of retardance at each pixel as shades of gray, while the orientation of birefringence is displayed as a series of lines (see Figure S2 and Supplemental Experimental Procedures) [20–22]. Calibration of the slow

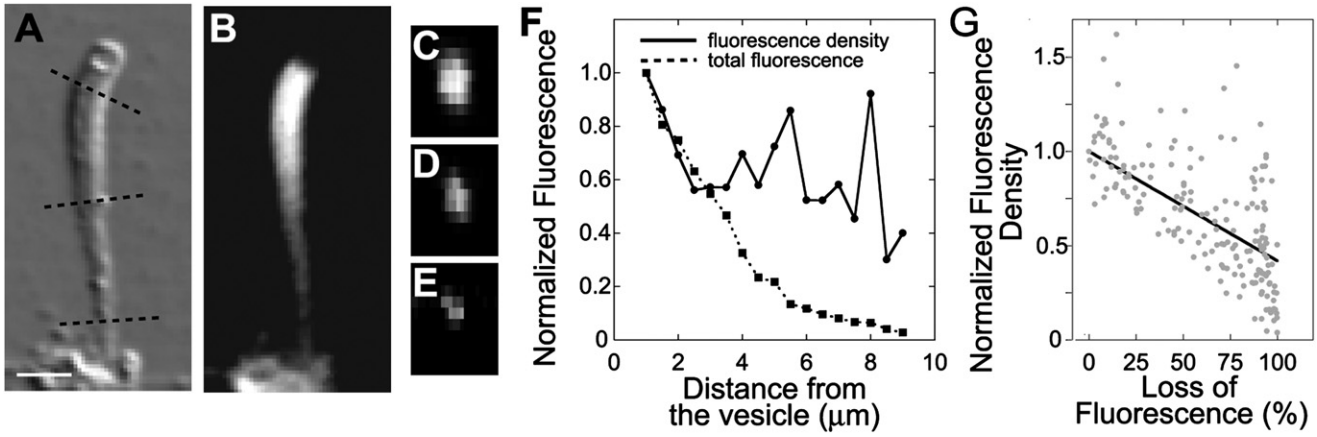

Figure 2. Filament Packing Density Is Partially Conserved during Retraction

(A) Differential interference contrast image of a comet tail fiber grown in the presence of Cy3-MSP. Scale bar represents 2 μm.

(B) The same fiber viewed by confocal fluorescence microscopy. The fiber is shown as a projection of a stack of images through the z axis.

(C–E) Cross-sections at the positions indicated by the dashed lines in (A). The images were generated from the same z stack used to produce (B). Linear contrast adjustment was applied to make all pixels containing fluorescent signal visible.

(F) Changes in the total filament mass (dotted line) and the relative filament density (solid line) at selected points along the length of the comet tail fiber. Total filament mass was calculated as the total fluorescence intensity in arbitrary units in all pixels within each cross-section of the fiber. The relative filament density was determined by dividing the total fluorescence intensity by the area of the cross-section. That area was determined by using EM images to measure the radius of the fiber at each position where a cross-section was obtained and then calculating its cross-sectional area. Both total filament mass and relative filament density were normalized to the values obtained for a cross-section near the front of the fiber and plotted against distance from the vesicle.

(G) Plot of normalized relative filament density versus the percent loss of fluorescence (100 − normalized total fluorescence) for 194 cross-sections obtained from eight fibers. The solid line is a plot of the linear regression. Note that even when the total filament mass in cross-sections is almost completely gone, the fibers retain ~45% of their filament density.

axis of birefringence using arrays of MSP filaments of known orientation showed that the orientation of birefringence generated by LC-PolScope microscopy parallels the long axis of the MSP polymer (Figure S2).

To determine whether the pattern of birefringence orientation in fibers changed during retraction, we captured successive images of a specific region of a comet tail fiber as it underwent retraction (Figure 4A). The boxed region shown in this sequence was not retracting at the start of this interval but had nearly completed retraction by the end. Initially, much of the birefringence in this region was oriented approximately normal to the fiber axis, with much less oriented axially (Figure 4B). As this region began to retract, its retardance decreased and its birefringence orientation shifted toward the fiber axis (Figure 4A). The fraction of axis-aligned pixels (those within 15° of the long axis) increased more than 4-fold (Figure 4C), and we observed orientation parallel to the axis at 110 s that was not present earlier (Figure 4B). Thus, the change in the birefringence pattern is not due to selective survival of axis-aligned filaments and, instead, fiber retraction involves an active rearrangement of at least some of the surviving of filaments.

Mechanism of Motor-Independent Retraction

Although actomyosin contraction contributes to cell body retraction in some crawling cells [5], several recent reports have shown that cells can still crawl when their myosin activity is compromised [6–9]. These observations suggest that motor-based contraction may not account completely for retraction even in actin-based cells. Sun and colleagues [23] have elaborated a mechanism for generating contraction that does not require the mechanochemical activity of conventional motor proteins. According to this model, the free energy of a filament network is minimized when the entropic contribution based on filament dispersion is balanced by enthalpic energy resulting from attractive interactions between filaments; that is, the network has an optimum packing density. This model envisions that depolymerization of filaments will reduce the packing density of the network so that it becomes suboptimal. Provided that that the interaction between filaments is transient, the remaining filaments will move closer together (thus increasing the packing density) so that the overall energy of the system decreases until the enthalpic gain and entropic loss balance. Thus, minimizing the energy of the filament network causes it to contract to its optimum packing density.

The relatively constant packing density observed along retracting MSP fibers provides direct experimental evidence to support an optimum packing model and suggests the following mechanism for depolymerization-mediated retraction in comet tail fibers. Retraction starts with catastrophic depolymerization of individual filaments. As filament loss proceeds, the interactions between the filaments decrease, allowing them to move more freely. The resulting increase in the movement of the surviving filaments would result in collisions between filaments and the formation of new interactions. As a result, the filament network in the fiber would tend to rearrange spontaneously, bringing filaments closer together to restore the packing density to its optimum value. Consistent with this hypothesis, as comet tail fibers retract, >90% of filament mass is lost, but ~50% of their preretraction packing is retained. Mathematical modeling of MSP fiber disassembly and retraction as a comparable two-step process involving filament detachment from the network followed by

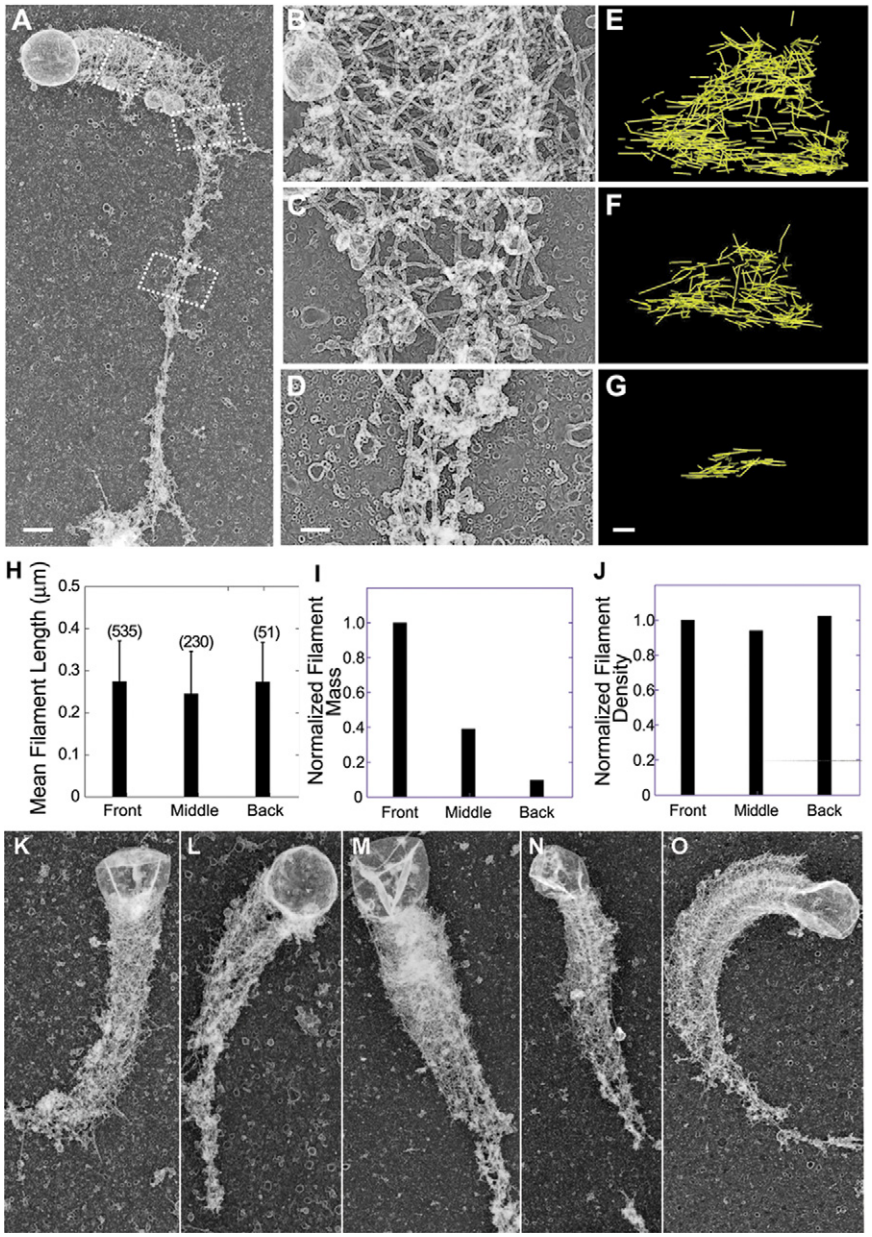

Figure 3. Platinum-Carbon Replica and Electron Tomograms of Comet Tail Fibers

(A) Panoramic view of a comet tail fiber. Scale bar represents 1 μm.

(B–D) Higher-magnification views of three regions of identical length from the nonretracting front (B), actively retracting middle (C), and nearly completely retracted rear (D) of the comet tail fiber in (A). Scale bar represents 200 nm.

(E–G) Cross-sectional views of 3D models produced by tracking the filaments (yellow) in the regions shown in (B–D), respectively, in tomographic reconstructions of the fiber. The view shown is a cross-section looking down the fiber axis from the forward face of each region.

(H) Graph showing the average filament length in tomograms in (E–G). The numbers of filaments measured are in parentheses. Error bars represent one standard deviation.

(I) Total filament mass within each of the three tomograms, determined as the number of filaments in each normalized to number in the front region tomogram.

(J) Filament density in tomograms, determined as the total number of filaments divided by the volume, which was estimated as the filament-containing area of the cross-section multiplied by the length of the tomogram along the comet tail axis.

(K–O) A gallery of comet tail fibers. Note that each shows the same general organization, in which the diameter narrows from about the middle of the fiber rearward and the surviving filaments in this region are tightly packed.

depolymerization [24] predicts a strikingly similar retention of 50% of initial packing density in the fiber. This conservation of filament packing density with progressively fewer filaments would cause the network to shrink and pull the rear part of the network and any attached objects forward. In crawling sperm, disassembly of the cytoskeleton occurs at the base of the lamellipod where it joins the cell body [13]. Although the way in which the cell body is mechanically coupled to the MSP cytoskeleton has not been defined, shrinkage of the cytoskeletal network like that observed in comet tail fibers could pull the cell body forward. This mechanism is consistent with mathematical modeling of *C. elegans* sperm locomotion, which predicts that disassembly-induced cytoskeletal stress can account for cell body retraction [25].

Although our results were obtained using the specialized *Ascaris* sperm (MSP) motility system, the principles identified here are likely to also be applicable to more general actin-based cell motility. Our results highlight how a pulling force can be generated by filament depolymerization and rearrangement without the necessity for motor proteins, consistent with recent work indicating that such mechanisms may also be important in actin-based cells [9]. Moreover, our results provide empirical evidence to support the proposal [23] that balancing enthalpic interaction and entropic dispersion of filaments within a network can power retraction in amoeboid cells.

Supplemental Information

Supplemental Information includes two figures, Supplemental Experimental Procedures, and four movies and can be found with this article online at doi:10.1016/j.cub.2011.08.047.

Acknowledgments

We thank Lori McFadden for expert technical assistance, Kim Riddle and Tom Fellers of the Biological Science Imaging Resource at Florida State

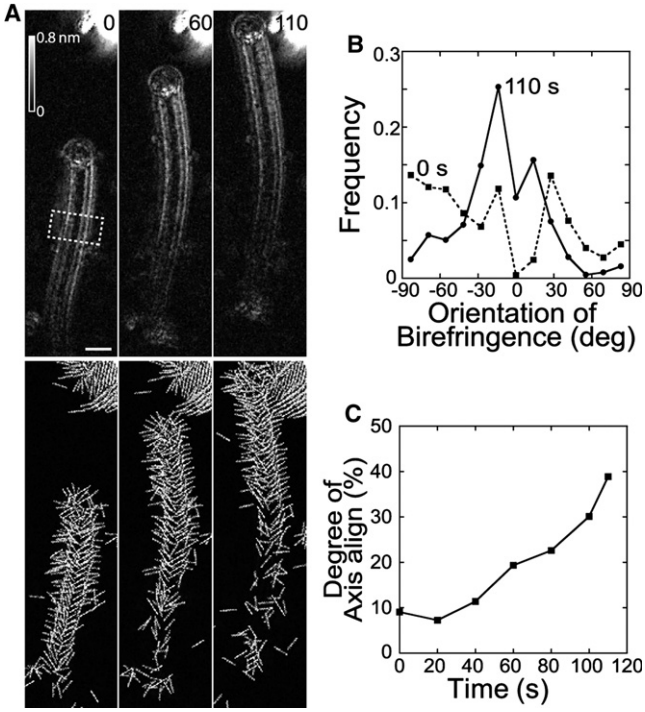

Figure 4. Rearrangement of Filaments during Fiber Retraction Detected by LC-PolScope Microscopy

(See Figure S1 for an explanation of LC-PolScope-computed images.)

(A) Time-lapse sequences of retardance (upper) and slow axis orientation (lower) images. Numerals indicate elapsed time in seconds. Scale bar represents 2 μm. In the retardance images, the magnitude of retardance at each pixel is shown as shades of grade according to the scale at the upper left. In the lower set of panels, the orientation of the slow axis of birefringence at every fifth pixel is displayed as a line. Note that the lines do not represent individual filaments.

(B) Plot of the relative frequency distribution of orientation lines in the boxed region in (A) at 0 and 110 s. The plots were generated from 708 and 162 data points for 0 and 110 s, respectively.

(C) Graph showing the percentage of orientation lines in the boxed region in (A) within ±15° of the fiber axis over time. See also Figure S2.

University for assistance with electron and confocal microscopy, and Rudolph Oldenbourg at the Marine Biological Laboratory for valuable assistance with and access to his instrumentation for polarization microscopy. This work was supported by the National Institutes of Health (NIH; R37-GM29994). N.N. was supported by an NIH grant (R01-EB002583) to Rudolf Oldenbourg.

Received: July 22, 2011
Revised: August 16, 2011
Accepted: August 17, 2011
Published online: October 13, 2011

References

1. Rafelski, S.M., and Theriot, J.A. (2004). Crawling toward a unified model of cell mobility: spatial and temporal regulation of actin dynamics. Annu. Rev. Biochem. *73*, 209–239.
2. Small, J.V., and Resch, G.P. (2005). The comings and goings of actin: coupling protrusion and retraction in cell motility. Curr. Opin. Cell Biol. *17*, 517–523.
3. Pollard, T.D., and Cooper, J.A. (2009). Actin, a central player in cell shape and movement. Science *326*, 1208–1212.
4. Pollard, T.D., and Borisy, G.G. (2003). Cellular motility driven by assembly and disassembly of actin filaments. Cell *112*, 453–465.
5. Vicente-Manzanares, M., Ma, X., Adelstein, R.S., and Horwitz, A.R. (2009). Non-muscle myosin II takes centre stage in cell adhesion and migration. Nat. Rev. Mol. Cell Biol. *10*, 778–790.
6. Knecht, D.A., and Loomis, W.F. (1987). Antisense RNA inactivation of myosin heavy chain gene expression in *Dictyostelium discoideum*. Science *236*, 1081–1086.
7. De Lozanne, A., and Spudich, J.A. (1987). Disruption of the *Dictyostelium* myosin heavy chain gene by homologous recombination. Science *236*, 1086–1091.
8. Mogilner, A., and Keren, K. (2009). The shape of motile cells. Curr. Biol. *19*, R762–R771.
9. Wilson, C.A., Tsuchida, M.A., Allen, G.M., Barnhart, E.L., Applegate, K.T., Yam, P.T., Ji, L., Keren, K., Danuser, G., and Theriot, J.A. (2010). Myosin II contributes to cell-scale actin network treadmilling through network disassembly. Nature *465*, 373–377.
10. Italiano, J.E., Jr., Stewart, M., and Roberts, T.M. (2001). How the assembly dynamics of the nematode major sperm protein generate amoeboid cell motility. Int. Rev. Cytol. *202*, 1–34.
11. Roberts, T.M., and Stewart, M. (2000). Acting like actin. The dynamics of the nematode major sperm protein (msp) cytoskeleton indicate a push-pull mechanism for amoeboid cell motility. J. Cell Biol. *149*, 7–12.
12. Bullock, T.L., McCoy, A.J., Kent, H.M., Roberts, T.M., and Stewart, M. (1998). Structural basis for amoeboid motility in nematode sperm. Nat. Struct. Biol. *5*, 184–189.
13. Italiano, J.E., Jr., Stewart, M., and Roberts, T.M. (1999). Localized depolymerization of the major sperm protein cytoskeleton correlates with the forward movement of the cell body in the amoeboid movement of nematode sperm. J. Cell Biol. *146*, 1087–1096.
14. Italiano, J.E., Jr., Roberts, T.M., Stewart, M., and Fontana, C.A. (1996). Reconstitution in vitro of the motile apparatus from the amoeboid sperm of Ascaris shows that filament assembly and bundling move membranes. Cell *84*, 105–114.
15. Miao, L., Vanderlinde, O., Stewart, M., and Roberts, T.M. (2003). Retraction in amoeboid cell motility powered by cytoskeletal dynamics. Science *302*, 1405–1407.
16. Yi, K., Wang, X., Emmett, M.R., Marshall, A.G., Stewart, M., and Roberts, T.M. (2009). Dephosphorylation of major sperm protein (MSP) fiber protein 3 by protein phosphatase 2A during cell body retraction in the MSP-based amoeboid motility of Ascaris sperm. Mol. Biol. Cell *20*, 3200–3208.
17. Cameron, L.A., Svitkina, T.M., Vignjevic, D., Theriot, J.A., and Borisy, G.G. (2001). Dendritic organization of actin comet tails. Curr. Biol. *11*, 130–135.
18. Waterman-Storer, C.M., Desai, A., Bulinski, J.C., and Salmon, E.D. (1998). Fluorescent speckle microscopy, a method to visualize the dynamics of protein assemblies in living cells. Curr. Biol. *8*, 1227–1230.
19. Kueh, H.Y., Brieher, W.M., and Mitchison, T.J. (2010). Quantitative analysis of actin turnover in *Listeria* comet tails: evidence for catastrophic filament turnover. Biophys. J. *99*, 2153–2162.
20. Oldenbourg, R., and Mei, G. (1995). New polarized light microscope with precision universal compensator. J. Microsc. *180*, 140–147.
21. Oldenbourg, R. (1996). A new view on polarization microscopy. Nature *381*, 811–812.
22. Katoh, K., Hammar, K., Smith, P.J., and Oldenbourg, R. (1999). Birefringence imaging directly reveals architectural dynamics of filamentous actin in living growth cones. Mol. Biol. Cell *10*, 197–210.
23. Sun, S.X., Walcott, S., and Wolgemuth, C.W. (2010). Cytoskeletal cross-linking and bundling in motor-independent contraction. Curr. Biol. *20*, R649–R654.
24. Wolgemuth, C.W., Miao, L., Vanderlinde, O., Roberts, T., and Oster, G. (2005). MSP dynamics drives nematode sperm locomotion. Biophys. J. *88*, 2462–2471.
25. Zajac, M., Dacanay, B., Mohler, W.A., and Wolgemuth, C.W. (2008). Depolymerization-driven flow in nematode spermatozoa relates crawling speed to size and shape. Biophys. J. *94*, 3810–3823.